Gas-phase photocatalytic activity of sputter-deposited anatase TiO_2 films: Effect of <001> preferential orientation, surface temperature and humidity

B. I. Stefanov, G. A. Niklasson, C. G. Granqvist, L. Österlund*

Department of Engineering Sciences, The Ångström Laboratory,
Uppsala University, P.O. Box 534, SE-751 21 Uppsala, Sweden

Abstract

We present a systematic *in situ* study of the environmental reaction conditions on the photocatalytic activity of sputter deposited anatase TiO_2 films with controlled amounts of preferential <001> orientation. In particular, the effects of relative humidity (RH) and substrate temperature (T^{surf}) are investigated. It is found that {001} facets, which are present in higher abundance on highly oriented samples, exhibit an order of magnitude higher reactivity for gas-phase photocatalytic oxidation of the indoor air pollutant acetaldehyde (CH_3CHO) than {101} facets do, and a functional dependence of the reaction rate on facet orientation is determined. It is proposed that water adsorbed on the film contributes with two counteracting effects on the photocatalytic activity: (*i*) It provides hole acceptors to complete the photo-induced redox cycle and subsequent $OH^{\cdot}$ radical formation for pollutant degradation, and (*ii*) it creates a diffusion barrier between the catalyst interface and pollutant molecules adsorbed in the water layer. As a consequence, increasing T^{surf} at high RH has the beneficial effect of removing excess water and reducing the diffusion barrier, thereby improving the photocatalytic activity. A comparison is also made with a commercial anatase TiO_2 film, with less developed surface crystallinity and random facet distribution, where the improvement is even more pronounced. Films with a higher degree of orientation exhibit much more stable performance over a range of operating conditions, which suggests that it is possible to tune the effects of water and exposed facet orientation to achieve optimum activity and making TiO_2 films amenable to a larger (RH, T^{surf}) parameter space for practical applications.

Keywords: TiO_2, photocatalysis, acetaldehyde, <001> orientation, surface temperature, humidity, *in situ* reaction kinetics

* Corresponding author: lars.osterlund@angstrom.uu.se

1. Introduction

Anatase TiO_2 thin films are widely used as photo-catalysts in environmental applications, such as for water and air cleaning [1; 2], and they are also employed as self-cleaning surfaces [3; 4; 5]. Such films are utilized in numerous commercial products, and a large number of related scientific reports are published (about 9,000 in the past 5 years, according to the ISI Web of Knowledge]) [6]. Current topics in the field include ways to improve photocatalytic efficiency, visible light activity and stability/durability and embrace various doping strategies [7; 8], physical and chemical methods to modify the surface [9; 10] and, recently, crystal-facet engineering [11; 12; 13]. There is ample evidence that the reactivity of the normally less abundant {001} surfaces is higher than that of the usually dominating {101} [14; 15]. The {001} surfaces constitute around 10% of the exposed crystal area in randomly oriented TiO_2 nanocrystals, as dictated by bulk thermodynamics [16]. Most studies have hitherto focused on anatase nanoparticles, prepared by wet-chemical synthesis, whose crystallographic structure can be altered by hydrothermal synthesis and by F^--ion-assisted shape control [17]. There are much fewer studies on morphology-controlled anatase thin films prepared by physical vapour deposition. However, such studies are important because the latter methods are industrially viable and readily up-scalable for fabrication of robust catalyst films on a variety of substrates. Moreover, physical thin film deposition can open new vistas for preparing morphology-controlled anatase nanostructures which are not accessible via solution-based growth, as we have previously reported [18].

In this study we focus on anatase TiO_2 films with controlled <001> preferential orientations, prepared by magnetron sputter deposition, and explore the photocatalytic activity of these films for removal of an indoor air pollutant under a variety of environmental reaction conditions. It has been known for three decades that sputter-deposited films exhibit preferential <001> orientation under typical sputter conditions [19], and a number of approaches have been put forward to control this process [20; 21; 22; 23]. However, there is little data on the effects of preferential growth on the photocatalytic activity of TiO_2 films, especially under realistic operation conditions. We recently demonstrated a method to fine-tune the preferential orientation of sputter-deposited anatase TiO_2 films, specifically to alter the distribution of exposed crystallographic facets on the film surface, and we reported a functional dependence of the reactivity of those films for a liquid-phase photo-oxidation reaction of Methylene Blue (MB) [18]. Here we expand these studies and present results on the effect of preferential <001> orientation on gas-phase photocatalytic degradation of the common indoor pollutant acetaldehyde [24; 25; 26; 27] for various environmental conditions, specifically being substrate temperature (T^{surf}) and relative humidity (RH). Our present study aims at showing the applicability of facet-controlled TiO_2 films in reaction environments that mimic realistic conditions for photo-catalysts in the built environment.

2. Sample preparation and characterisation

2.1. Preparation of anatase TiO_2 films

TiO_2 films were deposited on 4-mm-thick glass substrates (70 x 70 mm iron-free OptiWhite glass, Pilkington) by reactive DC magnetron sputtering in a set-up based on a Balzers UTT 400 vacuum unit [28]. Deposition was made in Ar + O_2 process gas (20 mTorr total pressure) for 30 min with unheated substrates and using two 5-cm-diameter Ti targets (99.995%, Plasmaterials, CA, USA). The targets were used in tandem at a fixed sputtering current of 0.75 A, which resulted in a sputtering power in the range 238–294 W (proportional to the O_2 partial pressure P_{O2}). The only variable parameter was P_{O2}, which was adjusted from 0.64 to 1.81 mTorr in order to prepare five batches of samples. The films were post-annealed for 1 h at 500 ^{o}C in air. More information about the preparation process is given in our previous publications [18; 22; 23].

A commercial photocatalytic TiO_2 film on a glass substrate, again with 4 mm thickness (Pilkington Active^{TM}), was used as a reference in order to compare the photocatalytic activity of the sputter-deposited films with data from current TiO_2 film technology. The commercial film consisted of an approximately 15-nm-thick TiO_2 coating deposited by chemical vapour deposition [29].

2.2. Characterization

Phase composition and preferential orientation of the films were determined by Grazing-Incidence X-Ray Diffraction (GI-XRD) using a Siemens D5000 diffractometer, employing $CuK_{\alpha 1}$ radiation and 0.5° incidence angle. Figure 1 shows diffractograms obtained for diffraction angles (2θ) in the range 20–80°. As-deposited TiO_2 films were amorphous but transformed to single-phase anatase upon annealing. Crystallite sizes were found to be in the 19–25-nm range and were independent of P_{O2}.

An obvious sign for increased preferential orientation in the <001> direction, apparent in Figure 1, is the changing ratio between the intensities of the (004) and (101) reflections in Figure 1. The degree of preferential orientation was estimated by Rietveld refinement, using the PowderCell software package [30], and the March–Dollase (MD) texturing model [31]. This model is based on altering the calculated diffraction pattern for a film with random orientation with the MD distribution function, which gives the probability of finding a crystallite with the crystallographic direction of interest (in this case <001>) at a given angle to the direction of the film plane. This allows for a fitting parameter, called the MD parameter, to be obtained during the Rietveld refinement process. The MD parameter serves as a qualitative descriptor for the amount of <001> orientation. It allows estimations of both the excess of preferentially oriented crystallites (η_{001}) [32] and of the expected relative area of exposed {001} facets at the film's surface (A_{001}) [18]. Increasing P_{O2} from 0.65 to 1.82 mTorr resulted in an enhancement of η_{001} from 2 to 34% and a corresponding growth of A_{001} from 10 to 36, where 10% pertains to the {001} coverage in a film with randomly oriented nanocrystallites [16]. The procedure of obtained A_{001} and η_{001} for sputter-deposited TiO_2 films with preferential orientation is explained in greater detail in our previous publication [18].

Optical properties of the films were obtained from UV/Vis/NIR transmittance spectra taken in the 300–1200 nm range with a Perkin-Elmer Lambda 900 spectrophotometer. Swanepoel's envelope method [33] was used to determine refractive indices and film thicknesses. Packing densities of the films were determined from refractive indices by use of Pulker's equation [34]. Surface morphology and microstructure were analysed with atomic force microscopy (AFM), scanning electron microscopy (SEM), and transmission electron microscopy (TEM). For AFM, we employed a PSIA XE150 SPM/AFM instrument (Park Systems, Suwon, Korea) equipped with a silicon cantilever (ACTA, AppNano) and operated in non-contact mode. Surface and cross-sectional SEM micrographs were recorded on a FEI/Philips XL30 FEG ESEM instrument operated at 10 kV accelerating voltage in hi-vac mode. Cross-sectional micrographs were obtained by use of a JEOL 2000FX TEM operated at 200 kV. For TEM, we used a simple sample preparation technique wherein flakes from the sputter deposited film were scraped off and dispersed in chloroform; the flakes were then deposited on a holey-carbon TEM grid by dipping it in the suspension. The sputter deposited films exhibit columnar growth and easily split in the growth direction so that cross-sectional fragments are readily obtained.

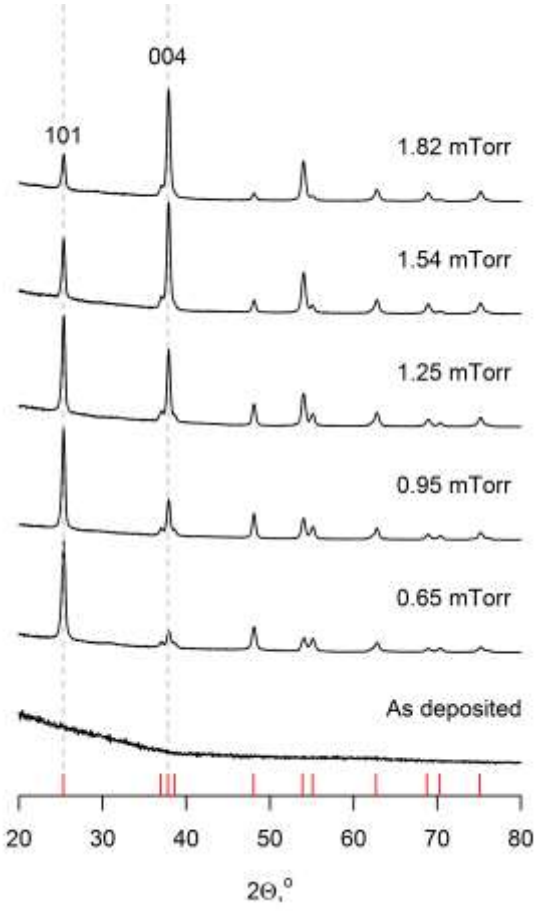

Figure 1. X-ray diffractograms for heat-treated crystalline TiO_2 films, prepared by sputtering at the shown values of P_{O2}, and a typical diffractogram for an amorphous as-deposited film. Characteristic peaks due to anatase TiO_2 are indicated by red bars.

2.3. Photocatalytic measurements and data treatment

Photocatalytic activity of the TiO_2 films was measured in a home-built flow-through reactor depicted in Figure 2. It comprises a gas-supply system, a reaction cell and a semiconductor sensor for volatile organic compounds (VOCs). The reaction cell consists of a stainless steel frame equipped with two identical glass windows, one of which is coated with the photocatalytic film. The windows are positioned 5 mm apart and sealed with silicone gaskets so that they enclose a volume of 12.5 mL and expose an active catalyst area of 50 x 50 mm. The cell is sandwiched between a heater, positioned behind the coated window to control the catalyst's surface temperature, and a UV light source facing the catalyst. A set of three UV LEDs (P8D136 70 mW high-intensity LED, wavelength 365 ± 5 nm, Seoul Optodevice, Korea) were arranged in a triangular geometry 120° apart and 11 mm from their common geometrical center as shown in Figure 3b. The control over the surface temperature was with a stability of 2°C and the feedback was provided via a DS18B20 1-wire digital thermometer IC (Maxim Integrated, CA, USA) placed inside the heater.

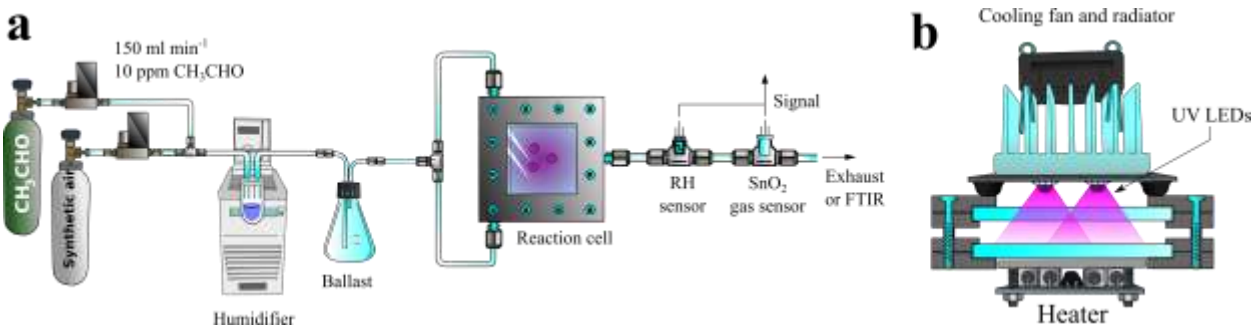

Figure 2. (a) Schematic of the set-up to measure photocatalytic CH_3CHO removal under dynamic conditions. (b) Side view of the reaction cell, showing positions of the light source and heater.

The gas-phase experiments used acetaldehyde, CH_3CHO (90 ppm in N_2, 99.99%, Air Liquide) mixed with synthetic air (N_2 and O_2 in lines with independent flow control, both 99.99%, from an in-house supply) and diluted to 10 ppm. The total flow rate was 150 ml min^{-1}, except for experiments with commercial Pilkington Active™ glass samples in which the flow was decreased to 100 ml min^{-1} due to the lower activity. For experiments conducted at RH > 0, the gas flow was passed through a glass bottle with deionized water, kept at constant temperature (± 0.1° K) in a water bath. A capacitance sensor (HIH-4000, Honeywell Inc., USA), positioned in the gas stream, was used for on-line monitoring of the relative humidity. The water bath temperature was adjusted to obtain desired RH values to an accuracy of 0.1%.

2.3.1. Spatial light intensity distribution

The spatial distribution of UV light intensity *I* over the catalyst was calculated from an angular distribution model for LEDs, suggested by Moreno [35], according to

$$I(\theta) = \sum_{i=1}^{3} a_i \cos(\theta - b_i)^{c_i} \quad . \qquad (1)$$

If the LED is approximated as a point source, the angular distribution of its relative intensity $I(\theta)$ follows a cosine law, *i.e.*, $I(\theta) = I(0)\cos(\theta)$, and contributions from the LED's reflector and lens are approximated as a sum of cosine functions, each with three adjustable parameters denoted a_i, b_i and c_i. This sum was then fitted to the angular intensity distribution data supplied by the LED manufacturer as shown in Figure 3a [36]. The spatial intensity distribution for the LED array was finally calculated by displacing each of the three LEDs according to its position in an (x_j , y_j) array and is given by

$$I^{tot}(x,y,z) = \sum_{j=1}^{3} \frac{I_0}{z^2} I\left(\arctan\left(\frac{\sqrt{(x+x_j)^2+(y+y_j)^2}}{z}\right)\right) \quad , \qquad (2)$$

where the *z* coordinate is perpendicular to the irradiated surface of the catalyst and I_0 is a constant.

Figure 3b depicts the calculated spatial distribution of the UV light intensity over the catalyst. The average UV illumination intensity was found to be 13 mW cm^{-1}, with local values ranging from 10 to 20 mW cm^{-1}. It was suggested by Mills *et al*. [37] that the effect of photocatalytic oxidation on the UV intensity has three regions: a linear dependence at very low illumination intensity, square root dependence at medium intensity, and independence of the illumination intensity at high intensity. In a previous study of liquid-phase photo-oxidation of MB [22], we observed that sputter deposited samples with thicknesses similar to those in the present work approached the saturation region at intensities as low as 0.4 mW cm^{-1}, so we can safely conclude that the intensity will not play a crucial role for comparisons of the catalyst activity for the different films under the current conditions.

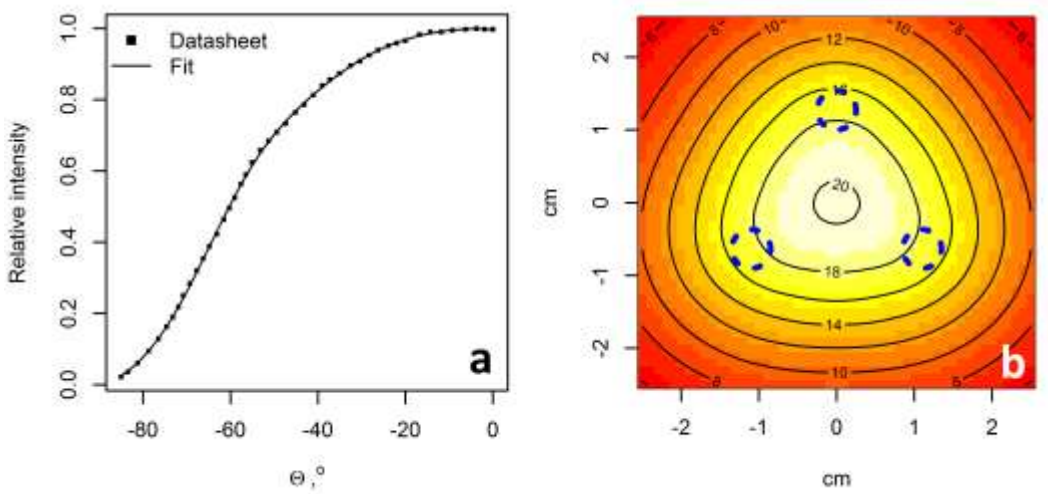

Figure 3. (a) Angular distribution of relative UV light intensity from a single LED according to the manufacturer's specification, and a fit of these data by use of Moreno's model [35]. (b) Positions of the three UV LEDs in an array (blue dashed circles) and ensuing spatial light distribution over the exposed catalyst surface with iso-intensity lines indicated (in mW/cm^{-2}).

2.3.2. Measurement of CH_3CHO concentration

The acetaldehyde concentration, C_{CH_3CHO}, was measured in the exit gas stream by a semiconductor gas sensor (HS-130AS, Sencera Co., Taiwan) which recorded the voltage V_{CH_3CHO} across a shunt resistor coupled in series with the sensing element. Each experiment lasted for 4 h and 45 min and consisted of three periods with increasing T^{surf} (25, 40 and 55°C), each with three 15-min-long UV illumination periods and intermittent 15-min dark periods for self-calibration; see Figure 4a. The experiments were then repeated at different values of RH, without regenerating the sample between the measurements, in order to elucidate dynamic effects of the external conditions on the photocatalytic activity. Figure 4b shows an unprocessed gas sensor signal which is related to C_{CH_3CHO} and can be converted to reaction rate. Dips in V_{CH_3CHO} represent the 15-min UV illumination periods. The slight changes in V_{CH_3CHO} for consecutive cycles is due to deactivation and reactivation processes in the catalyst, associated with changing numbers of blocked and active surface sites, as further discussed below.

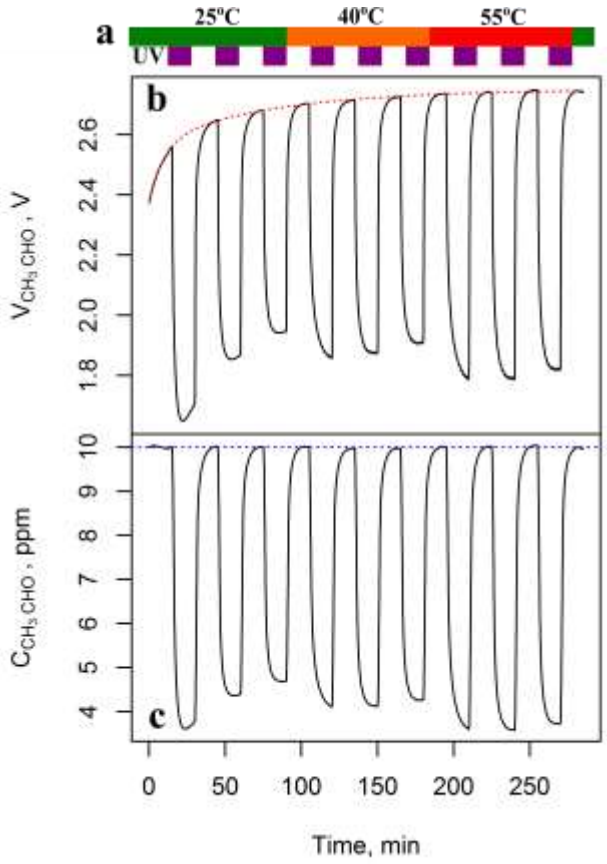

Figure 4. (a) Experimental sequence employed in the gas-phase photo-catalysis measurements; the same sequence was used for each relative humidity. (b) Experimental data on voltage V_{CH3CHO} across a shunt resistance before data treatment and (c) on acetaldehyde concentration C_{CH3COH} after data treatment.

As $C_{\mathrm{CH_3CHO}}$ increases, the sensor's resistance is decreased, which yields a larger current through the sensor and a higher voltage across a shunt resistor. A functional dependence between $C_{\mathrm{CH_3CHO}}$ and $V_{\mathrm{CH_3CHO}}$ can be deduced via a calibration procedure, and to this end one must first correct for signal drift. The CH_3CHO concentration at the inlet is always 10 ppm during the dark periods, and therefore V_{CH_3CHO} should remain stable, but a slow drift of the gas sensor's resistance takes place during the course of each experiment and gives rise to a drift of the data. However, this drift follows a predictable pattern and can be compensated by a simple fitting to a polynomial function during the dark periods, as indicated by the dashed red curve in Figure 4b. We performed a number of calibration runs for 0–60 ppm of CH_3CHO and found $V_{\mathrm{CH_3CHO}}$ to be linearly proportional to $\sqrt{C_{\mathrm{CH_3CHO}}}$. The background signal at $C_{\mathrm{CH_3CHO}} = 0$ is less than 70 mV and negligible compared to the value 2.5–3 V at $C_{\mathrm{CH_3CHO}} = 10\ \mathrm{ppm}$. A calibration at RH = 40% showed that the humidity has a minor effect on $V_{\mathrm{CH_3CHO}}$ and does not affect the functional dependence between $V_{\mathrm{CH_3CHO}}$ and $C_{\mathrm{CH_3CHO}}$. Hence the voltage signal was converted to concentration through

$$C_{\mathrm{CH_3CHO}}\,[ppm] = \left(\frac{{V_{\mathrm{CH_3CHO}}}^2}{{V^{10\ \mathrm{ppm}}_{\mathrm{CH_3CHO}}}^2}\right) \times 10\ [\mathrm{ppm}]. \qquad (3)$$

2.3.3. Calculation of photocatalytic performance

Figure 4c presents data on $C_{\mathrm{CH_3CHO}}$. A steady-state rate constant for CH_3CHO removal, denoted $r_{\mathrm{CH_3CHO}}$, was obtained from the concentration measured at the end each 15-min UV illumination cycle (the timing of the cycles is indicated on Figure 4a); this procedure was used to accommodate for the response time of the sensor, which is about 7 min. $r_{\mathrm{CH_3CHO}}$ was then derived from the drop of $C_{\mathrm{CH_3CHO}}$ content in the exhaust flow according to

$$r_{\mathrm{CH_3CHO}}[\,\mu\ \mathrm{mol\ min^{-1}cm^{-2}}] = \frac{(10\ [\mathrm{ppm}] - C_{\mathrm{CH_3CHO}}\ [\mathrm{ppm}])}{10\ [\mathrm{ppm}]S[cm^2]}\ F\ [\,\mu\ \mathrm{mol\ min^{-1}}], \qquad (4)$$

where *S* is the exposed coated area of the catalyst (25 cm^2), and *F* is the CH_3CHO flow rate, which was 0.061 µmol min^{-1} and 0.041 µmol min^{-1} for total flow rates of 150 mL min^{-1} (oriented films) and 100 mL min^{-1} (commercial film), respectively.

To determine how the reaction rate varies under changing environmental conditions, three contributions were calculated and are presented as relative changes of $r_{\mathrm{CH_3CHO}}$. The first of these is the change within the three UV illumination cycles at fixed conditions, which is defined as $\Delta r_{\mathrm{CH_3CHO}}$ and obtained from

$$\Delta r_{\mathrm{CH_3CHO}} = \frac{(r^{(3)}_{\mathrm{CH_3CHO}} - r^{(1)}_{\mathrm{CH_3CHO}})}{r^{(1)}_{\mathrm{CH_3CHO}}} \times 100\ [\%], \quad (5)$$

where $r^{(3)}_{\mathrm{CH_3CHO}}$ and $r^{(1)}_{\mathrm{CH_3CHO}}$ are the rates observed during the third and first UV illumination cycle, respectively , and is a measure of the intrinsic change of reaction rate during repeated photo-oxidation. At RH = 0, this contribution reflects the catalyst deactivation that is normally observed for anatase TiO_2 [38]. In our previous study on CH_3CHO photo-degradation kinetics of commercial TiO_2 powders, we observed that there are two types of active sites on the surface, which exhibit different activity, and that the relative fraction of highly active sites decreases when the catalysts is degraded [10]. The other two parameters, $\Delta r^{\mathrm{RH}}_{\mathrm{CH_3CHO}}$ and $\Delta r^{T}_{\mathrm{CH_3CHO}}$, indicate the change in $r_{\mathrm{CH_3CHO}}$ when RH and T^{surf}, respectively, are varied relative to dry conditions and room temperature (T = 25°C), which are usually the reported conditions in the literature, and are given by

$$\Delta r^{T}_{\mathrm{CH_3CHO}} = \frac{(r^{T}_{\mathrm{CH_3CHO}} - r^{T=25^\circ\mathrm{C}}_{\mathrm{CH_3CHO}})}{r^{T=25^\circ\mathrm{C}}_{\mathrm{CH_3CHO}}} \times 100\ [\%] \quad (6)$$

and

$$\Delta r^{\mathrm{RH}}_{\mathrm{CH_3CHO}} = \frac{(r^{\mathrm{RH}}_{\mathrm{CH_3CHO}} - r^{\mathrm{RH=0\%}}_{\mathrm{CH_3CHO}})}{r^{\mathrm{RH=0\%}}_{\mathrm{CH_3CHO}}} \times 100\ [\%]\,. \quad (7)$$

2.3.4. FTIR measurements

The VOC gas sensor does not discriminate between different organic species and is unable to detect the presence of gas-phase intermediates. The possible existence of such intermediates were recorded by use of Fourier transform infrared (FTIR) spectroscopy, specifically in experiments wherein the exhaust gas from the cell was transported through a long-path FTIR gas cell (Model 8-PA, Infrared Analysis Inc., Anaheim, CA, USA) with sensitivity to CH_3CHO in the ppb regime; spectra were taken at the beginning and end of each UV illumination cycle. Two FTIR spectra of this kind are shown in Figure 5. Both of them were corrected in order to remove spectral distortions from the δ(HOH) water band, which is caused by small amounts of water vapor in the gas cell due to the photo-oxidation reaction or associated with trace amounts of water contaminating the supply of synthetic indoor air. This correction is important because the δ(HOH) band overlaps partly with the carbonyl frequency region in CH_3CHO.

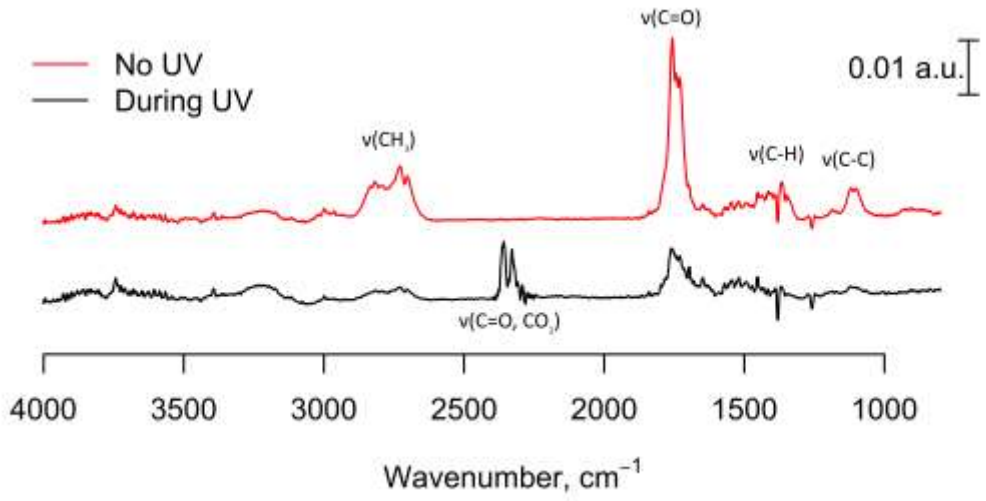

Figure 5. FTIR spectra of gas-phase CH_3CHO before and during UV illumination. The spectrum during UV illumination was obtained at the end of a 15-min-long UV illumination cycle, which allowed sufficient time that the FTIR gas cell would be saturated with reaction products. The data display characteristic features due to the shown vibration modes in CH_3CHO and CO_2.

Figure 5 shows evidence for nothing but CH_3CHO. Its amount is reduced during UV illumination, and there is a concomitant production of gas-phase CO_2. We note that the presence of CO_2 cannot be detected with the gas sensor. Gas-phase water production from the photo-oxidation is not evident in the spectra, which is a consequence of the compensation algorithm applied to eliminate effects of residual water in the synthetic gas stream.

In two previous studies we have reported the detailed reaction mechanism of adsorption and photocatalytic oxidation of CH_3CHO on the surface of nanoparticulate TiO_2 films [10; 39]. The major reaction intermediates were found to be crotonaldehyde, which is a product of the aldol condensation of CH_3CHO during its adsorption on the surface, which is then converted to surface-bound formate during the photooxidation reaction. A number of other surface intermediates—such as HCOOH, CH_3CH_2OH, *etc*., have also been reported in the literature [40]. Gaseous intermediates, however, were not apparent in the FTIR data presented in Figure 5. Hence, it is concluded that CH_3CHO is completely mineralized during the reaction, and any intermediates in the gas-phase are below the detection limit, *i.e*., no larger than in the low ppb regime.

3. Results and discussion

3.1. Morphology and preferred crystallographic orientation

Figures 6 and 7 present SEM top views and cross-section, a TEM cross-sectional image and AFM images of sputter deposited TiO_2 films, and Table 1 summarizes process parameters and physical properties of the films. No morphology differences were observed for samples prepared at different

values of P_{O2}. The AFM surface roughness was consistently found to be of the order of 2 nm. Film thicknesses lay in the 700–900-nm range and were larger in samples made at higher P_{O2}, *i.e.*, the sputter rate increased slightly with increasing P_{O2}. The refractive index decreased linearly with enhanced P_{O2}, from 2.22 to 2.05, this is related to a slight decrease in the packing density by about 10%. In a previous study [18], we found that such a decrease probably is associated with the formation of enclosed pores that are inaccessible to the reactants during the photocatalytic reaction, and therefore the apparent enhancement of the surface area does not lead to increased reaction rates. In general, the films can be regarded as crystalline and having pronounced columnar growth morphology.

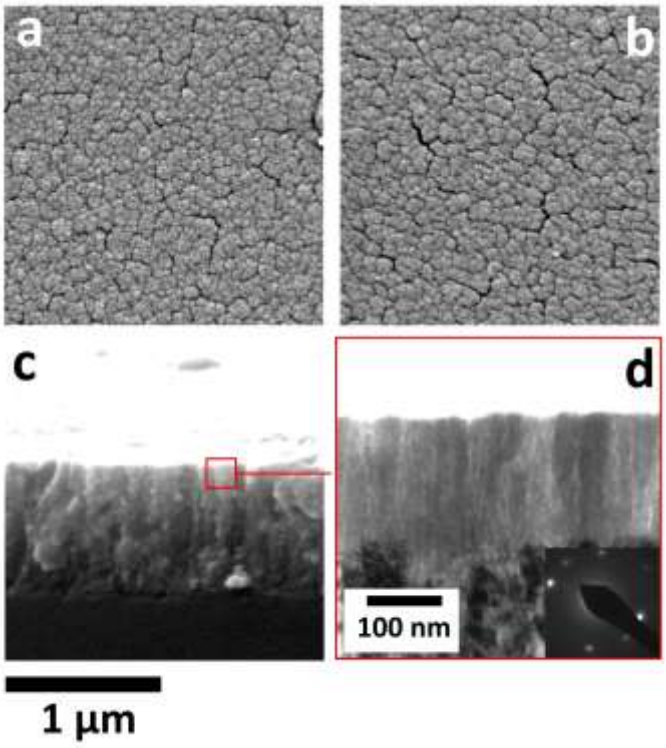

Figure 6. SEM micrographs showing surface morphologies of TiO_2 films deposited at P_{O2} being (a) 0.65 mTorr and (b) 1.82 mTorr. Representative cross-sectional images from (c) SEM and (d) TEM for a film with highly preferential orientation, prepared at P_{O2} = 1.82 mTorr. The inset in (d) shows a selected-area electron diffraction pattern and demonstrates the <001> preferred orientation.

The Pilkington Active™ coating consists of anatase TiO_2 with a low degree of crystallinity; it is backed by a protective SiO_2 coating whose role is to inhibit sodium ion diffusion from the glass substrate [29]. Our AFM characterisation revealed that the surface morphology was less developed than that of the sputter deposited films. Specifically $R_{rms.}$ was 0.9 nm for the Pilkington Active™ coating, whereas R_{rms} was 2 nm for the sputter deposited films, which implies that the commercial photo-catalyst has a lower effective area.

Table 1. Film deposition parameters and physical properties of anatase TiO_2 films. The various entries indicate partial oxygen pressure during deposition (P_{O2}), sputtering power (P), film thickness (t), sputtering rate (R), mean crystallite size ($\bar{d}_{XRD}$), March-Dollase parameter (MD), preferential <001> orientation (η_{001}), relative area of exposed {001} facets (A_{001}), root mean square AFM roughness (R_{rms}), refractive index (n), and packing density (PD).

P_{O2}, mTorr	P, W	t, nm	R, nm min^{-1}	$\bar{d}_{XRD}$, nm	MD	η_{001}, %	A_{001}, %	$R_{rms.}$, nm	n	PD, %
0.65	238	708	23.6	21	1.036	2	10	1.9	2.22	87
0.95	245	755	25.2	24	0.859	9	15	1.8	2.21	87
1.25	258	716	23.9	25	0.717	19	22	1.7	2.23	88
1.54	275	835	27.8	22	0.586	30	31	2.2	2.10	82
1.82	294	933	31.1	19	0.535	34	36	1.8	2.05	80

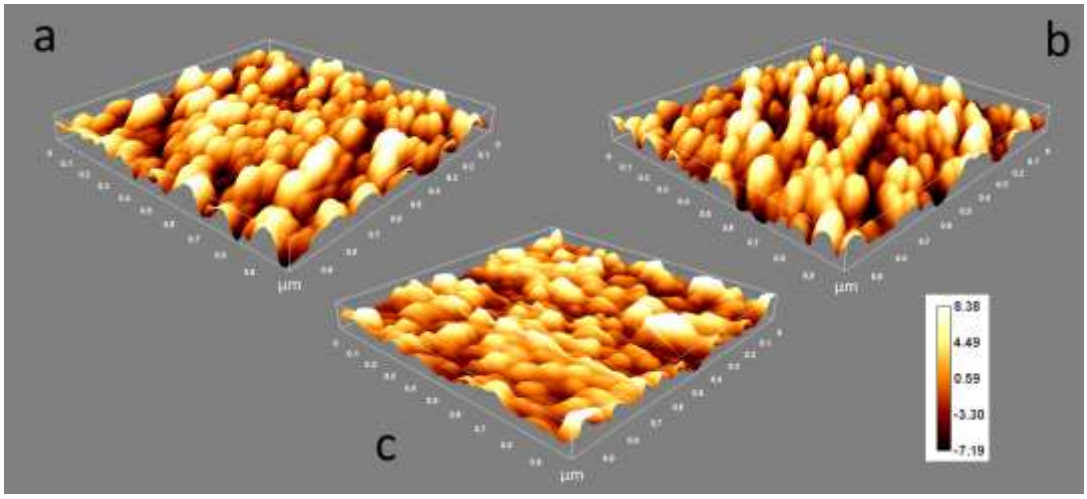

Figure 7. AFM images of TiO_2 films prepared by sputter deposition at P_{O2} being (a) 0.65 mTorr and (b) 1.82 mTorr. (c) AFM image of a Pilkington Active™ sample. The vertical scale is colour-coded.

3.2. Photocatalytic reaction rate

A quantitative functional dependence of r_{CH_3CHO} on A_{001} was established by using a simple model approximating the anatase TiO_2 surface as comprised of two types of sites associated with two types of crystal planes: highly reactive (001) facets, whose abundance is determined by A_{001}, and (101) facets which covers the rest of the surface. The higher concentration of Ti atoms on the (001) surface was accounted for by a factor f_{001} = ([Ti]$_{001}$/[Ti]$_{101}$) = 1.35, estimated from crystallographic data [18]. The model for the reaction rate then takes the form

$$r_{\mathrm{CH_3CHO}} = r_{101}(1 - A_{001})^x + r_{001}(f_{001}A_{001})^x \quad , \tag{8}$$

where r_{101} and r_{001} are the respective photocatalytic reaction rates on the two types of surface sites, and x is a parameter.

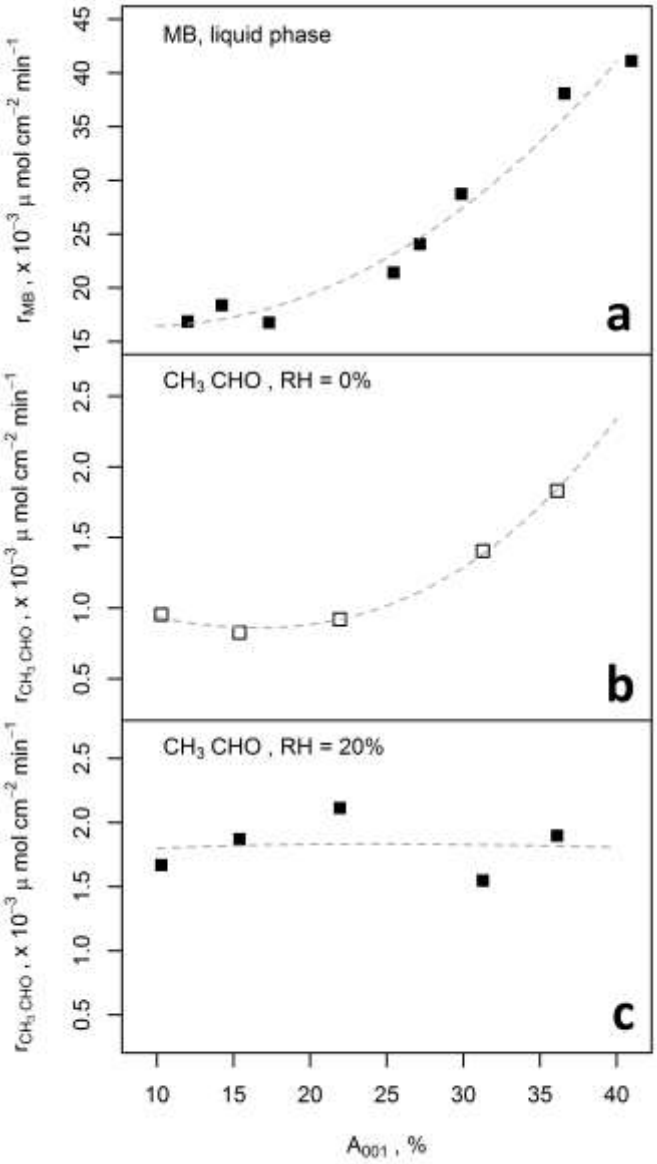

Figure 8. Effect of the amount of preferential <001> orientation on the photocatalytic rate constants of (a) Methylene Blue (MB) in liquid phase, as reproduced from our previous work [18], (b) CH_3CHO in gas-phase at RH = 0, and (c) CH_3CHO in gas-phase at RH = 20%. Dashed curves show model fits for (a) and (b), and dashed line in (c) is drawn to guide the eye. All data are for room temperature.

Figure 8b presents a fit of the gas-phase photo-oxidation reaction for acetaldehyde at RH = 0. These results are very similar to those for liquid-phase MB photo-oxidation, presented in our previous study [18] from which representative and recalculated data are shown in Figure 8a. For MB, we obtained $x \approx 2.12$ thus suggesting a quadratic dependence and $r_{001}/r_{101} \approx 8$. For gas-phase CH_3CHO photo-oxidation, on the other hand, we obtain $x \approx 3.04$ so that $r_{001}/r_{101} \approx 10$. In both cases the activity of the {001} facets is found to be close to an order-of-magnitude higher than the activity of the {101} facets, which normally dominate for bulk anatase TiO_2 crystals. The transition of the reaction order from quadratic to cubic indicates that x is related to the detailed reaction mechanism, for example to the difference of the adsorption energy of MB and CH_3CHO on the {101} and {001} surfaces, or to different intermediate reaction kinetics. The results suggest that controlled surface texturing of anatase TiO_2 films can be tailored for specific applications in order to achieve optimum reactivity. Further elucidation calls for detailed surface- science studies of crystal-facet-specific adsorbate-surface interactions.

Table 2. Rate constant (r_{CH3CHO}) for photocatalytic decomposition of acetaldehyde on sputter deposited TiO_2 films with different amounts of preferential <001> orientation, as represented by A_{001}, and analogous data for a commercial Pilkington Active™ photocatalytic film on glass. Data is given for different values of surface temperature (T^{surf}) and relative humidity (RH).

	r_{CH3CHO}, µmol CH_3CHO cm^{-2} min^{-1} (x 10^{-3})								
	RH = 0			RH = 20%			RH = 40%		
T^{surf}, °C / A_{001}, %	25 °C	40 °C	55 °C	25 °C	40 °C	55 °C	25 °C	40 °C	55 °C
10	0.954	1.073	1.297	1.669	1.912	2.084	1.694	1.765	1.954
15	0.826	0.933	1.081	1.870	2.052	2.173	1.741	1.792	1.948
22	0.921	0.995	1.162	2.114	2.207	2.277	2.115	2.032	2.108
31	1.404	1.520	1.660	1.548	1.705	1.809	1.388	1.618	1.698
36	1.831	1.936	2.028	1.897	2.017	2.078	1.542	1.766	1.847
Pilkington	0.014	0.014	0.015	0.012	0.019	0.023	0.016	0.031	0.051

The functional dependence of the photocatalytic rate constant on A_{001} was found to be valid only at RH = 0, and changing RH was shown to drastically influence r_{CH3CHO}. Figure 8c reveals that all samples exhibited similar activities at RH = 20%, regardless of A_{001}. Analogous results were observed at RH = 40%, albeit with a slightly lower rate constant at all values of A_{001}. Data for various magnitudes of T^{surf} and RH are listed in Table 2 for the complete set of films with different A_{001} values and analogous data for a commercial Pilkington Active™ film. Data for a few values A_{001} and the commercial TiO_2 film are plotted in Fig. 9 to illustrate the trends apparent in Table 2. The data demonstrate that r_{CH_3CHO} are significantly increased for films with low A_{001} as a function of RH and somewhat more at RH = 20% than at RH = 40%. In contrast, r_{CH3CHO} for films with high A_{001} remains similar regardless of T^{surf} and RH; the reaction rate is high and of the same magnitude, or higher, than for films with low values of A_{001}

regardless of which T^{surf} and RH are employed. The commercial Pilkington Active™ film was found to exhibit two orders-of-magnitude lower reaction rates than for the sputter deposited samples—which we attribute to its low crystallinity and small surface area (as quantified by the lower value of R_{rms}). The apparent dramatic increase of r_{CH_3CHO} seen for the commercial catalyst at high T^{surf} and RH, may indicating that hydroxyl concentration and product desorption are limiting the reactivity of the commercial film to a much larger extent that the sputtered films. We note, however, that the measurement accuracy is about 2 x 10^{-6} μmol cm^{-2} min^{-1}, and hence the relative error is larger for the measurements on the commercial film which exhibit much lower values of r_{CH_3CHO}.

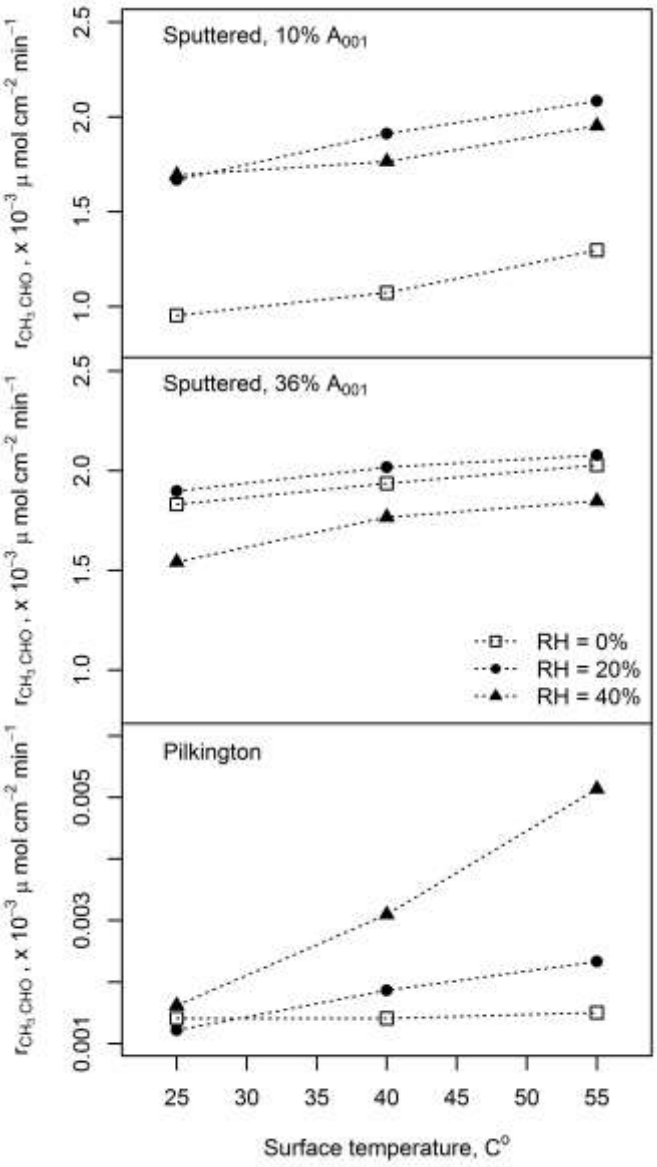

Figure 9. Photocatalytic reaction rate r_{CH_3CHO} at different surface temperature and relative humidity (RH) for sputter deposited TiO_2 films with the shown degree of preferential orientation (A_{001}) and for a commercial Pilkington Active™ sample. Symbols

represent data and lines are drawn to guide the eye. The accuracy of the measured $r_{\mathrm{CH_3CHO}}$ values is about 2 x 10^{-6} µmol cm^{-2} min^{-1}.

It is known that the relative humidity critically influence the photocatalytic reaction rate [38; 41; 42]. Under dry conditions, the reactivity of the surface itself is important, and the formation of strongly bound intermediates can inhibit the binding of reactant molecules so that the photo-catalyst is deactivated when operated at room temperature [43]. Water is beneficial to the photocatalytic reaction for two reasons: (*i*) it acts as a hole-scavenger that completes the redox cycle at the catalyst interface whereby electrons reduce oxygen and holes oxidize water/hydroxyls, and (*ii*) it generates hydroxyl radicals which promote the degradation of organic pollutants. While the photo-generated electron–hole pairs can oxidize the adsorbed contaminants directly, this reaction must take place within their lifetime, which is of the order of hundreds of ps [44]. In contrast, the lifetimes of $OH^{\cdot}$ radicals is an order-of-magnitude longer and extends into the ns range [45]. However, the formation of water layers on the catalyst—which readily takes place at room temperature and for standard pressure in a humid atmosphere—creates a diffusion barrier which may impede mass-transport of radicals. Transport of the pollutant molecule through the water layer can also be a limiting factor, which depends on the solubility of the molecules of interest in water. In fact, it is known that water can be an inhibiting factor for non-polar substrate molecules, with an example being the adsorption of acetone and chlorobenzene on TiO_2 where, respectively, a negligible and a suppressing effect was observed when water was present on the surface [46; 47]. In the present case, we note that CH_3CHO is water soluble and should be able to penetrate the surface water layer through diffusion. In Fig. 9a and b it is evident that $r_{\mathrm{CH_3CHO}}$ decreases as RH increases from 20 to 40%, which indicates that diffusion is limiting the reaction in those cases. From Fig. 9 it is seen that increasing T^{surf} results in an enhanced r_{CH_3CHO} in all cases, but that it has much less than RH. This strongly hints that radical generation is limiting the reaction rate, rather than product desorption, and we attribute the slight increase versus temperature seen in Fig. 9 due to the secondary effect of smaller water coverage at higher temperatures. Figure 10 summarizes the mechanisms that are proposed to govern the dependence of T^{surf} and RH on the photocatalytic degradation of acetaldehyde on TiO_2 thin films.

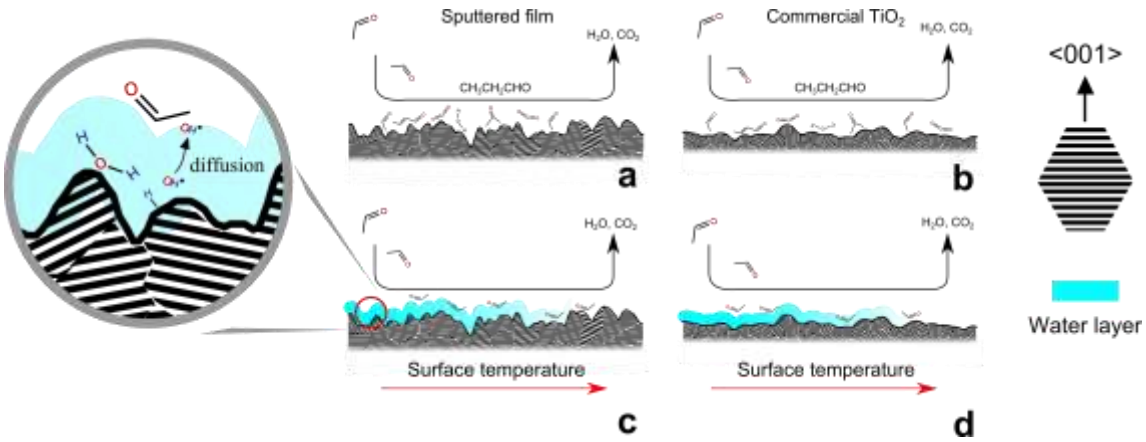

Figure 10. Schematic illustration of the effects of surface temperature (T^{surf}) and relative humidity (RH) on the photocatalytic reactivity for acetaldehyde ($r_{\mathrm{CH_3CHO}}$) of (a, c) sputter deposited and (b, d) commercial thin films of TiO_2. Under dry conditions (a, b), an increase of T^{surf} enhances $r_{\mathrm{CH_3CHO}}$ by boosting the desorption rates of CO_2 and H_2O, which are the reaction products. At RH > 0 (c, d) an increased value of T^{surf} diminishes the water layer and speeds up diffusion of photo-generated radicals, as illustrated in the left-hand inset. Surface morphology and crystalline structure also play roles, and the commercial sample is expected to have less efficient binding of reactants and intermediates as a result of its poor crystallinity and undeveloped surface texture.

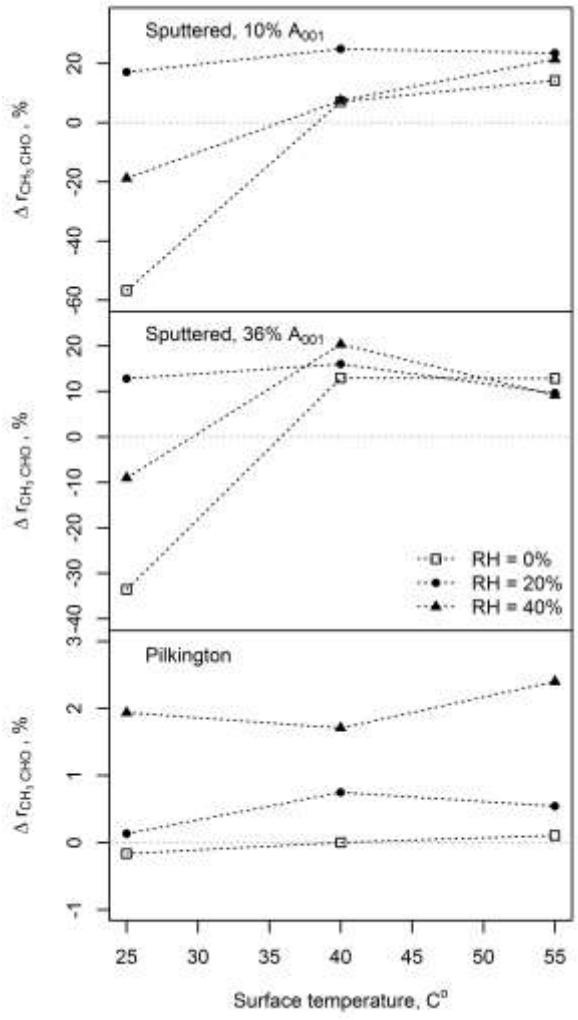

Figure 11. Change of the photocatalytic reaction rate $\Delta r_{\mathrm{CH_3CHO}}$ between successive cycles of UV irradiation, recorded at different surface temperature and relative humidity (RH), for sputter deposited TiO_2 films with the shown degree of preferential orientation (A_{001}), and analogous data for a commercial Pilkington Active™ sample. Symbols represent data and lines were drawn for convenience.

We now discuss the effect of deactivation as a function of cycle number and what effects RH and T^{surf} have on this. An indication that hydroxyl radicals play an important role for preventing deactivation in our experiments at RH > 0 can be obtained from the relative change of the reaction rate

constant during the cycles under fixed operation conditions, *i.e.*, during deactivation of the catalyst, which can be deduced from the data by means of Equations 5. At RH = 0%, $r_{\mathrm{CH_3CHO}}$ is found to decrease throughout the three reaction cycles, which can be reconciled with *in situ* surface micro-kinetic studies [10] which have revealed that there is an accumulation of intermediates on the surface, primarily as surface-bound CO_2, as well as creation of formate species. Plotting the deactivation, $\Delta r_{\mathrm{CH_3CHO}}$, given by Equation 5, *vs*. T^{surf} reveals an interesting dependence on RH, and Figure 11 presents such data for three cases: A film without preferential orientation (A_{001} = 10%), a film with strong preferential orientation represented by A_{001} = 36%, and the commercial Pilkington Active™ sample. Table 3 shows the effect of T^{surf} and RH on the relative change of $r_{\mathrm{CH_3CHO}}$ for the complete set of TiO_2 films with different A_{001} as calculated by Equations 6 and 7.

Table 3. Relative change in photocatalytic reaction rate ($\Delta r_{\mathrm{CH3CHO}}$) for acetaldehyde over sputter deposited TiO_2 films, with different preferential orientations (A_{001}), and for a commercial sample (Pilkington Active™). Data are shown for $\Delta r^{T}_{\mathrm{CH_3CHO}}$ at T = 55 °C (relative to 25 °C) and for $\Delta r^{\mathrm{RH}}_{\mathrm{CH_3CHO}}$ at different values of the relative humidity (RH), relative to RH=0%, at a fixed catalyst temperature T^{surf} = 25 °C.

	$\Delta r^{T=55\,°C}_{\mathrm{CH_3CHO}}$, % (Eq. 6)			$\Delta r^{\mathrm{RH}}_{\mathrm{CH_3CHO}}$, % (Eq. 7) ($T^{\mathrm{surf}}$ = 25°C)	
A_{001}, %	RH = 0%	RH = 20%	RH = 40%	RH = 20%	RH = 40%
10	36	25	15	75	78
15	31	16	12	126	111
22	26	8	0	129	130
31	18	17	22	10	-1
36	11	9	20	4	-16
Pilkington	9	90	215	-9	18

As expected, the sputter deposited samples exhibited deactivation during the first cycles of UV irradiation under dry condition, and Figure 11 shows that this effect was most pronounced for the sample with a low value of A_{001}. Increasing the humidity to RH = 20% led to re-activation of all samples ($\Delta r_{\mathrm{CH_3CHO}} > 0$), even at T^{surf} = 25 °C, which can be attributed to the effect of $OH^{\cdot}$ radicals produced under humid conditions. Table 3 demonstrates that films with low A_{001} displayed the strongest re-activation. A possible reason for this effect is the different affinity of {001} and {101} facets towards reduction and oxidation reactions, as reported in previous studies [48; 49]. At RH = 0 and at RH = 20%, we observed that the films with low A_{001} were affected to a higher extent by T^{surf} than the films with preferential <001> orientation. At RH = 40%, the positive effect of increasing T^{surf} is significant at T^{surf} = 40 °C. Increasing the catalyst temperature to T^{surf} = 55 °C resulted in only a minor increase of $\Delta r_{\mathrm{CH_3CHO}}$ (at small A_{001}) or even a slight decrease (at high A_{001}). The difference between films with low and high A_{001} is consistent with a notion that more reaction products are accumulated on films with low A_{001}, and the same notion can also explain why films with high A_{001} were less affected by

deactivation. At RH = 40%, the effect of T^{surf} was similar for all films probably because, at this condition, the role of the water layer thickness becomes the limiting factor.

4. Conclusions

We presented results on photocatalytic oxidation of gas-phase acetaldehyde by anatase TiO_2 films with controlled amounts of preferential <001> orientation. Films with a large fraction of exposed {001} facets exhibited higher activity than randomly oriented films exposing predominantly {101} facets; this difference prevailed for a range of reaction conditions, specifically for different catalyst temperature and relative humidity. We demonstrated that these ambient conditions influenced the activity of such films strongly. An optimum situation exists when there is a sufficient amount of water to facilitate electron–hole separation and $OH^{\cdot}$ radical formation but not so much water that it introduces limitations for the diffusion of reactants and reaction products. These conditions were outlined, in general terms, in a previous publication [50], but our discovery here—that the reactivity of different crystalline facets have different functional dependence as the relative humidity is altered—is new and suggests that different reaction mechanisms govern acetaldehyde oxidation on (001) and (101) facets.

We further showed that an increase of the catalyst temperature enhanced the photocatalytic activity, whereas the effect of modified relative humidity depends sensitively on the catalyst surface, *i.e.*, the exposed crystal surface. The presence of water may serve either to enhance or limit the photocatalytic activity depending on the reaction conditions and morphology of the catalyst. Notably the sputter deposited films with preferred <001> orientation are found to be much more tolerant towards changes in reaction conditions than such films with random orientation and also than commercial TiO_2 photo-catalyst films with less developed crystallinity.

Finally, we conclude that anatase TiO_2 films with carefully tuned preferential <001> orientation may find applications both as a model photo-catalyst, for elucidating effects of the crystalline structure on the reactivity under various situations, and as a practical photocatalytic coating when high activity is desired across a large range of operating conditions. We emphasize that the facet control of the TiO_2 films in this study was accomplished by properly selecting the conditions for magnetron sputtering, which is a readily up-scalable and industrially viable thin film deposition technique.

5. Acknowledgements

This work was funded by the European Research Council under the European Community's Seventh Framework Program (FP7/2007-2013)/ERC Grant Agreement No. 267234 ("GRINDOOR").

References

[1] D. Goswami, J. Sol. Energy Eng. 125 (2003) 359-365.
[2] O. Legrini, E. Oliveros, A. M. Braun, *Chemical Reviews* 93 (1993) 671-698.
[3] Y. Ohko, Y. Utsumi, C. Niwa, T. Tatsuma, K. Kobayakawa, Y. Satoh, Y. Kubota, A. Fujishima J. Biomed. Mater. Res. 58 (2001) 97-101.
[4] I. Parkin, R. Palgrave, J. Mater. Chem 15 (2005) 1689-1695.
[5] Y. Ohko, S. Saitoh, T. Tatsuma, A. Fujishima, J. Electrochem. Soc. 148 (2001)B24-B28.
[6] A. Mills, S.-K. Lee, J. Photochem. Photobiol. A 152 (2002) 233-247.
[7] J. C. Yu, J. Yu, W. Ho, Z. Jiang, L. Zhang, Chem. Mater. 14 (2002) 3808-3816.
[8] Y.-J. Xu, Y. Zhuang, X. Fu, J. Phys. Chem. C 114 (2010) 2669-2676.
[9] S. Yin, Q. Zhang, F. Saito, T. Sato, Chem. Lett. 32 (2003) 358-359.
[10] Z. Topalian, B.I. Stefanov, C.G. Granqvist, L. Österlund, J. Cat. 307 (2013) 265-274.
[11] E. Grabowska, M. Diak, M. Marchelek, A. Zaleska, Appl. Cat. B 156-157 (2014) 213-235.
[12] F. Pan, K. Wu, H. Li, G. Xu, W. Chen, Chem. Eur. J. 20 (2014) 15095-15101.
[13] N. Sutradhar, A. K. Biswas, S. K. Pahari, B. Ganguly, A.B. Panda, Chem. Commun. 50 (2014) 11529-11532.
[14] X.-Q. Gong, A. Selloni, J. Phys. Chem. B, 109 (2005) 19560-19562.
[15] M.V. Dozzi, E. Selli, Catalysts, 3 (2013) 455-485.
[16] U. Diebold, Surf. Sci. Rep. 48 (2003) 53-229.
[17] H.G. Yang, C.H. Sun, S.Z. Quiao, J. Zou, G. Liu, S.C. Smith, H.M. Cheng, G.Q. Lu, Nature 453 (2008) 638-641.
[18] B.I. Stefanov, G.A. Niklasson, C.G. Granqvist, L. Österlund, J. Mat. Chem. A 3(2015) 17369-17375.
[19] D.G. Howitt, A.B. Harker, J. Mater. Res. 2 (1987) 201-210.
[20] K. Eufinger, D. Poelman, H. Poelman, R. De Gryse, G.B. Martin, J. Phys. D 40 (2007) 5232.
[21] P. Singh, D. Kaur, Physica B 405 (2010) 1258-1266.
[22] B. Stefanov, L. Österlund , Coatings 4 (2014) 587-601.
[23] B. Stefanov, C.G. Granqvist, L. Österlund, J. Phys. Conf. Ser. 559 (2014) 012011.
[24] N. Gonzalez-Flesca, A. Cicolella, M. Bates, E. Bastin, Env. Sci. Pollution Res. 6 (1999) 95-102.
[25] B.F. Yu, Z.B. Hu, M. Liu, H.L. Yang, Q.X. Kong, Y.H. Liu, Int. J. Refrigeration 32 (2009) 3-20.
[26] G. Leonardos, D. Kendall, N. Barnard, J. Air. Pollution Control Asooc. 19 (1069) 91-95.
[27] D. Grosjean, A. H. Miguel, T. M. Tavares, Atmosph. Environ. B 24 (1990) 101-106.
[28] D Le Bellac, G.A. Niklasson, C.G. Granqvist, J. Appl. Phys. 77 (1995) 6145.
[29] I.P. Parkin, R.G. Palgrave, "CVD of Functional Coatings in Glass", editors A. C. Jones and M. L. Hitchman. "*Chemical Vapour Deposition: Precursors, Processes and Applications"* 2008, RSC , 451-476.
[30] W. Kraus, G. Nolzeb, J. Appl. Crystallogr. 29 (1996) 301.
[31] W.A. Dollase, J. Appl. Cryst. 19 (1986) 267-272.
[32] E. Zolotoyabko, J. Appl. Cryst. 42 (2009) 513-518.
[33] R. Swanepoel, J. Phys. E: Sci. Instrum. 16 (1983) 1214-1222.
[34] H.K. Pulker, Appl. Optics 18 (1979) 1969-1977.
[35] I. Moreno, C.-C. Sun, Optics Express 16 (2008) 1808-1819.
[36] Seoul Optodevice, P8D1 datasheed (available on a supplier website). https://www1.elfa.se/data1/wwwroot/assets/datasheets/P8D1_Serie_eng_tds.pdf , last accessed 6 Oct 2015.
[37] A. Mills, J. Wang, D.F. Ollis, J. Phys. Chem. B 110 (2006) 14386-14390.
[38] L. Österlund, " Vibrational spectroscopy of pure and doped TiO_2 photocatalysts". editor L. Vayssieres in "*On Solar Hydrogen and Nanotechnology* Wiley & Sons, 2009.

[39] B. Stefanov, Z. Topalian, C.G. Granqvist, L. Österlund, J. Mol. Catal. A 381 (2014) 77-88.

[40] M. D. Hernandez-Alonso, I. Tejedor-Tejedor, J. M. Coronado, M. A. Anderson, J. Soria, Cat. Today 143 (2009) 364-373.
[41] C. Hägglund, B. Kasemo, L. Österlund, J. Phys. Chem. B 109 (2005) 10886.
[42] A.V. Vorontsov, D.V. Kozlov, P.G. Smirniotis, V.N. Parmon, Kinetics and Catalysis 46 (2005) 422-436.
[43] D.V. Kozlov, A.V. Vorontsov, P.G. Smirniotis, Appl. Cat. B 42 (2003) 77-87.
[44] Y. Nosaka, M.A. Fox, J. Phys. Chem. 92 (1988) 1893.
[45] W.A. Pryor, Ann. Rev. Physiol. 48 (1986) 657-667.
[46] M.L. Sauer, D.F. Ollis, J. Catal. 149 (1994) 81-91.
[47] L. Zhang, W.A. Anderson, S. Sawell, C. Moralejo, Chemosphere 68 (2007) 546-553.
[48] T. Tachikawa, S. Yamashita, T. Majima, J. Am. Chem. Soc. 133 (2011) 7197.
[49] S.K. Wallace, K.P. McKenna, J. Phys. Chem. C 119 (2015) 1913.
[50] L. Österlund, ”Optimizing photocatalytic oxidation for purifying air”, SPIE Newsroom, 2006. DOI: 10.1117/2.1200608.0328